THE JOURNAL OF PHYSICAL CHEMISTRY C

Article

pubs.acs.org/JPCC

Panchromatic Solar-to-H_2 Conversion by a Hybrid Quantum Dots–Dye Dual Absorber Tandem Device

Victoria González-Pedro,[†] Isaac Zarazua,[‡] Eva M. Barea,[†] Francisco Fabregat-Santiago,[†] Elder de la Rosa,[‡] Iván Mora-Seró,*[,†] and Sixto Giménez*[,†]

[†]Photovoltaics and Optoelectronic Devices Group, Departament de Física, Universitat Jaume I, 12071 Castelló, Spain

[‡]Centro de Investigaciones en Optica, A.P. 1-948 Leon, Gto., 37150, Mexico

Supporting Information

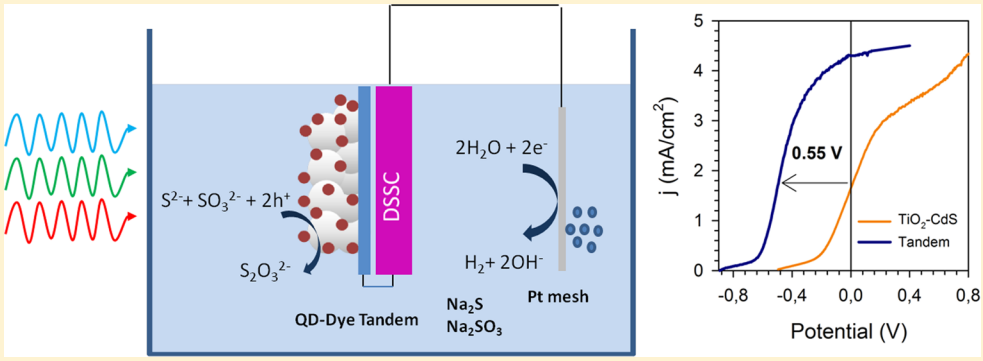

ABSTRACT: Solution-processed mesoscopic oxide semiconductor-based materials offer potentially low-cost and high stability alternative for next generation of water to hydrogen conversion photoelectrochemical cells (PEC). In the present study, we demonstrate the effective unassisted H_2 generation by a tandem device based on a quantum dot (QD)–dye dual absorber system. These systems are constituted by a TiO_2 mesoscopic photoanode sensitized with CdS QDs and a dye sensitized solar cell (DSSC), based on ruthenium dye, connected in series. This solar cell supplies the needed photovoltage to induce photodriven hydrogen production. Opto-electrochemical characterization of the single components allows the prediction of the operational photocurrents and a reliable estimation of the theoretical power conversion efficiencies of tandem systems. Evolved hydrogen under simulated solar illumination was collected, and solar to hydrogen conversion efficiencies (STH) were obtained. The tandem devices have demonstrated high stability in aqueous medium and solar-to-hydrogen conversion efficiency of (0.78 ± 0.04)%, near tripling the efficiency of single QD based photoanodes. These results highlight the importance of the design of hybrid photoanodes combining the effect of different light absorbers working in parallel tandem devices for the development of efficient H_2 generation QD-based photoelectrochemical cells.

INTRODUCTION

Harnessing energy from sunlight has some unique advantages in terms of availability and environmental benefits, which makes solar energy the most convenient resource to power the planet in the coming years.[1,2] One of the most promising strategies for solar energy conversion and storage is based on mimicking the photosynthetic organisms that harvest and store solar energy in chemical bonds from abundant raw materials (water and carbon dioxide).[3,4] This approach is termed artificial photosynthesis and the most simple scheme is based on the photoassisted splitting of water with semiconductor materials to generate hydrogen (H_2) as an energy carrier.[5]

From the seminal studies of Honda and Fujishima on the electrochemical photolysis by TiO_2,[6] the scientific community has intensively focused on the development of suitable semiconductor materials and devices able to efficiently decompose water with the only input of sunlight.[7−10] The most advanced devices entail dual band gap tandem p/n photoelectrolysis cells, which can provide solar-to-hydrogen (STH) efficiencies of 15%.[11,12] So far, efficiencies of 12.4% have been reported for III−V semiconducting materials, although at the expenses of high cost and low stability.[13] Recently, Nocera et al. demonstrated an artificial leaf device based on a triple junction photovoltaic structure with earth-abundant catalysts and STH efficiencies close to 8%,[9] although its high cost severely limits further commercial application. In this context, mesoscopic metal oxides appear as a promising alternative for unassisted water splitting providing a wide prospect of low cost materials with attractive features. Although several metal oxides have been extensively studied, such as TiO_2, WO_3, and α-Fe_2O_3, none of these materials allows efficient STH conversion due to either too large bandgaps (TiO_2, WO_3) or inadequate

Received: November 8, 2013
Revised: December 16, 2013
Published: December 16, 2013

band alignment to split water and reduce H_2 (WO_3, α-Fe_2O_3).[14]

Sensitization of wide bandgap semiconducting materials like TiO_2 can provide a smart solution to overcome the limitations of poor light harvesting in the visible region.[15,16] Indeed, several recent studies have reported solar hydrogen devices based on wide bandgap semiconducting materials (TiO_2, ZnO) sensitized by chalcogenide quantum dots (QDs).[17−22]

Although chalcogenide based semiconductors are not able to carry out unassisted solar water splitting since they quickly photocorrode in aqueous solutions, this limitation can be overcome by the use of sacrificial agents, i.e., $NaSO_3$ or Na_2S. As a remarkable example, short circuit currents of 16 mA/cm^2 have been reported by employing inverse opal TiO_2 photoanodes sensitized with CdSe.[19] However, narrow band gap semiconductors, as PbS, have also been studied to harness IR photons for photoelectrochemical conversion.[18,21] A "quasi artificial leaf" based on TiO_2/PbS/CdS heterostructures has proven to produce hydrogen under simulated solar illumination at a rate of 4.30 mL·cm^{-2}·day^{-1} in the presence of a sacrificial oxidation agent. Moreover, one of the fundamental problems of these systems relates to the position of the conduction band edge, slightly above the H^+/H_2 electrochemical potential, which precludes the reduction of hydrogen at useful rates; unless an external voltage is applied. Indeed, very limited studies have reported effective light driven H_2 evolution without the assistance of a bias potential.

In this study, we demonstrate a remarkable photocurrent for unassisted H_2 evolution (4.3 mA·cm^{-2}) obtained by a dual absorber tandem cell constituted by a TiO_2−CdS photoanode connected in series with a DSSC, which provides the extra energy needed for efficient water reduction to H_2. Moreover, the spectral response of the device is analyzed and solar-to-hydrogen conversion efficiencies are calculated, providing a rationale context for the true performance of sacrificial water splitting devices and highlighting some of the limitations of these systems.

EXPERIMENTAL METHODS

The TiO_2/CdS photoelectrodes consist of 9 μm thick transparent films of interconnected titania nanoparticles (DSL 18-NRT, 20 nm average particle size) deposited on FTO glass (Pilkington TEC15, ∼15 Ω/sq resistance) by screen printing (0.25 cm^2). The films were sintered for 30 min at 450 °C to obtain a good electrical contact between nanoparticles, and the film thickness was measured by contact profilometry (Dektak 6 from Veeco). The FTO glass was previously coated by a compact layer of 150 nm TiO_2 deposited by spray pyrolysis of titanium(IV)bis(acetoacetonato) di(isopropanoxylate) and sintered at 450 °C for 30 min. The mesoporous TiO_2 electrodes were in situ sensitized by CdS QDs grown by succesive ionic layer adsorption and reaction (SILAR). For this purpose, a solutions of 0.05 M $Cd(CH_3COO)_2$ dissolved in ethanol and Na_2S 0.05 M in methanol/water (v/v = 1/1) were used. A single SILAR cycle consisted of 1 min dip-coating of the TiO_2 electrode into the cadmium solution (Cd^{2+}) and subsequently into the sulfide solutions, also during 1 min. After each dipping step in a precursor solution, the electrodes were thoroughly rinsed by immersion in the corresponding solvent in order to remove the excess of precursor. This procedure was repeated five times. After sensitization, all the samples were coated by a ZnS layer, by alternatively dipping into 0.1 M $Zn(CH_3COO)_2$ and 0.1 M Na_2S solutions for 1 min/dip, rinsing with Milli-Q ultrapure water between dips (2 cycles).

The DSSCs cells were fabricated as a sandwich type structure. A double-layer configuration was employed as working electrodes. On a FTO conducting glass, a 8 μm thick transparent layer (DSL 18NR-T, 20 nm average particle size) was first screenprinted and further coated by a 4 μm thick second layer of scattering titania particles (WERO-4, 300−400 nm particle size distribution), and the resulting photoelectrodes were sintered at 450 °C for 30 min to obtain a good electrical contact between the nanoparticles. The film thickness was also examined by a Dektack 6 profilometer from Veeco. For dye sensitization, a squared TiO_2 (0.25 cm^2) electrode was immersed into a 0.3 M N719 dye solution for 16 h. A mixture of acetonitrile and *tert*-butanol (v/v = 1/1) was used as solvent. The devices were assembled with a counter electrode (thermally platinized TCO), using a Surlyn (Dupont) thermoplastic frame (25 μm thick). A 0.6 M 1-methyl-3 propylimidazolium iodide, 0.5 M 4-*tert*-buthylpiridine, 0.03 M I_2, and 0.1 M guanidinium thiocianate in acetonitrile/valeronitrile (v/v = 85/15) redox electrolyte was introduced through a hole drilled in the counter-electrode that was subsequently sealed.

Structural characterization was performed by a JEOL JSM 7600F field emission transmission electron microscope (TEM), while the absorption spectra were recorded between 300 and 800 nm by a Cary 500 UV−vis Varian spectrophotometer. Photoelectrochemical measurements were performed in a two electrode configuration using a Pt mesh as counter electrode (Sigma Aldrich, 100 mesh) and 0.25 M Na_2SO_3 0.35 M Na_2S aqueous solution as electrolyte with sacrificial agent (approximately 12 mL solution was employed). No separator was used between anolyte and catholyte. For the tandem device, the DSSC was aligned with the TiO_2−CdS photoanode, which was wired to the platinum counterelectrode of the DSSC. All the contacts were isolated with nitrocellulose resin before dipping in the electrolyte. Three identical cells were tested for each reported parameter, and the experimental error is taken as the standard deviation. Cyclic voltammetries were recorded at scan rate of 50 mV/s under 100 mW/cm^2 Xe-lamp illumination using a FRA equipped PGSTAT-30 from Autolab and a Keithley 2612 system sourcemeter. The incident photon to current conversion efficiency (IPCE) measurements were performed employing a 150 W Xe lamp coupled with a computer-controlled monochromator; the photocurrent was measured using an optical power meter 70310 from Oriel Instruments, using a Si photodiode to calibrate the system. Faradaic efficiencies were determined by measuring the evolved H_2 gas in larger area devices (1.5 × 1.5 cm^2) with a graduated inverted buret. Prior to the experiments, the electrolyte was degassed in ultrasonic bath. Both current and gas collection were performed after 20 min of stabilization. To obtain the correct number of hydrogen moles, the hydrogen pressure was determined as follows:

$$P_{H2} = P_{atm} - \rho(T)gh - P_v(T) \quad (1)$$

where P_{atm} is the atmospheric pressure, $\rho(T)$ is the mass density of the electrolyte solution, g is the gravitational acceleration, h is the height difference between the levels of column liquids, and $P_v(T)$ is the water saturation pressure. The correction of water vapor pressure was performed ($P_v(T)$ = 23.68 mmHg = 0.031 atm).[23] The second parameter of the equation above $\rho(T)gh$ was also considered in the calculations,

dx.doi.org/10.1021/jp4109893 | J. Phys. Chem. C 2014, 118, 891−895

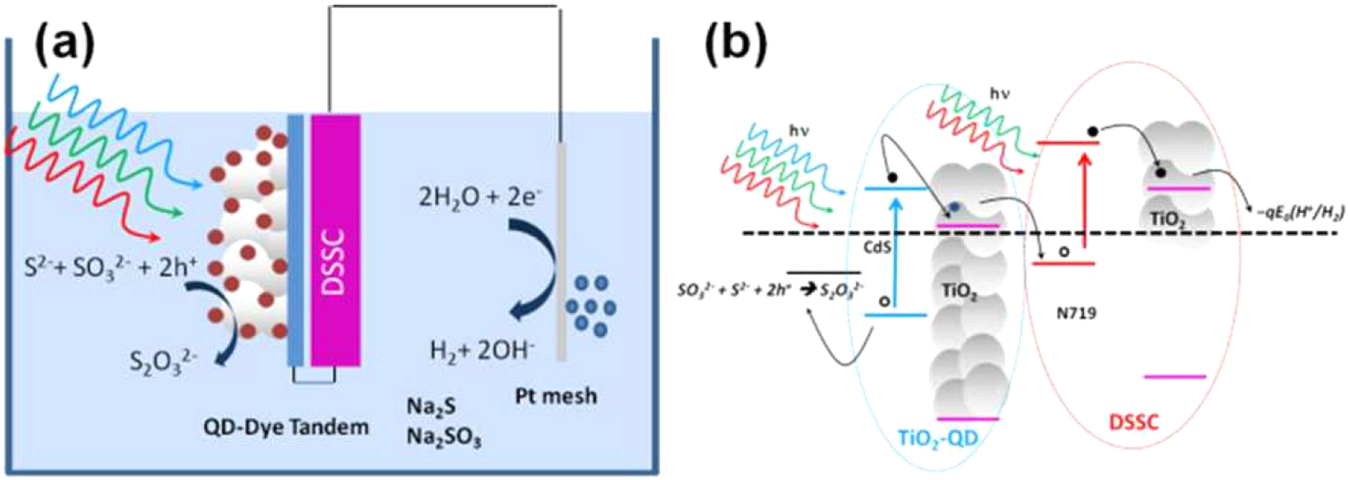

Figure 1. (a) Scheme of the two electrode photoelectrochemical cell and the measurement chamber. Reaction mechanisms for H_2 production are shown in the scheme. (b) Energy diagram illustrating the charge transfer phenomena in the PEC.

although its contribution to the total hydrogen pressure is marginal. A scheme of the device is shown as Figure S1, Supporting Information.

RESULTS AND DISCUSSION

For a dual absorber device, the optimal light harvesting conditions entail the maximization of the light absorption at both sensitizers. Consequently, CdS QDs and a DSSC device with the ruthenium 719 dye were selected since both sensitizers exhibit partially complementary absorption spectral ranges (see Figure S2, Supporting Information). Although from the absorption spectra shown in Figure S2, the bandgap of CdS is close to the bulk material (2.4 eV), the synthetic method employed here is generally used for the band gap tuning of CdS, and we kept the term "quantum dot" in the article.

A scheme of the device is presented in Figure 1a, and the energetics of the system is shown in Figure 1b. The light entering the photoelectrochemical cell first reaches the TiO_2/CdS photoanode, and upon visible absorption, an electron/hole pair is created at the CdS QD. Subsequently, the photogenerated electron is injected into the mesoporous TiO_2 structure, and after reaching the FTO substrate, it is directed toward the DSSC connected in series, which captures the remaining light of the initial beam and provides the additional bias to autonomously evolve hydrogen at the Pt cathode. On the other hand, the corresponding hole in the CdS QD is reduced by the sacrificial agent in the solution ($NaSO_3$).

Figure 2a,b shows the current−potential (j−V) curves and the incident photon to current efficiency (IPCE), respectively, of the individual components of the device: the photoanode (TiO_2−CdS) and the dye sensitized solar cell (DSSC). The DSSC was also tested with the QDs photoanode facing the light beam, although not connected, in order to evaluate the effect of TiO_2/CdS absorption on the DSSCs performance. As a consequence of the lower incident light, the DSSC performance drops 56.2% when immersed in the measurement chamber, and 32% in the presence of the QD photoanode (Table S1, Supporting Information). This reduction of incident (and thus absorbed) light in the DSSC due to the presence of CdS is mainly confined to the 300−500 nm region, as evidenced by the subtraction of both IPCE spectra (dashed pink line in Figure 2b).

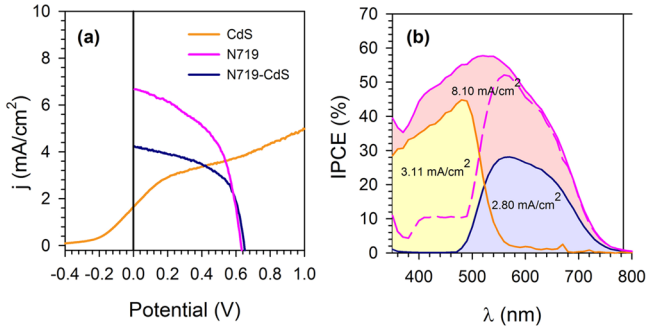

Figure 2. (a) j−V curves and (b) incident photon to current efficiency (IPCE) for CdS (solid orange), N719 (solid pink), and CdS plus N719 in series but not connected (solid blue). Dashed pink curve is obtained as $IPCE_{DSSC}$−$IPCE_{TiO2\text{-}CdS}$. The integrated currents are displayed under the IPCE area. The IPCE of QD based photoelectrode was recorded at applied potential of 0.7 V. The DSSCs was measured in the electrolyte to discard optical losses that can be attributed to the measurement chamber.

Despite the large decrease of both efficiency and photocurrents, 64% and 60%, respectively, in the DSSC as a consequence of the optical losses in the measurements chamber, the short-circuit current, j_{sc}, is high enough to facilitate tandem device operation, without charge transfer limitations from the TiO_2−CdS photoanode to the DSSC. The photocurrent of the TiO_2/CdS photoanode at zero bias is 1.64 ± 0.2 mA/cm^2, while the intersection point of single devices takes place at 3.48 mA/cm^2 (Figure 2a). This point provides a reasonable prediction of the operational current density for the tandem device, which is expected to significantly overperform the light driven current of the individual TiO_2/CdS photoanode (almost three times enhancement).

The maximum current for the different light absorbing systems was estimated by integration of the IPCE spectrum multiplied by the photon flux in the relevant wavelength range, and the obtained values are displayed under the shaded areas in Figure 2b. These integrated currents are in reasonable good agreement with those obtained from photoelectrochemical measurements. However, the estimated operational photocurrent of the tandem system (based on both light absorbing elements connected in series) is provided by the single light absorbing element, which provides the lowest current density.

dx.doi.org/10.1021/jp4109893 | J. Phys. Chem. C 2014, 118, 891−895

Consequently, the operational current for the tandem device is 3.11 mA/cm^2, see Figure 2b.

The next step was assembling the tandem device and testing its experimental performance. Current−voltage curves for both the TiO_2/CdS photoanode and the tandem cell are plotted in Figure 3. When connecting the DSSC in series, a 0.55 V

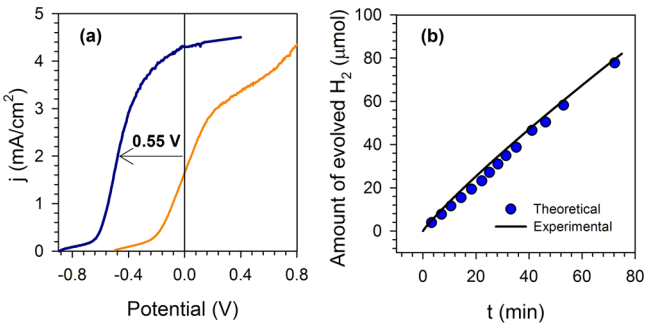

Figure 3. Current−voltage curves of the single TiO_2−CdS photoanode (orange) and tandem device with DSSC connected in series (blue). (b) Evolution of hydrogen gas during the experiment.

cathodic shift of the photocurrent onset is observed, attributed to the contribution of DSSCs, which promotes the electrons to a higher energy level and dramatically improves the performance for unassisted hydrogen generation. This cathodic shift is consistent with the photovoltage of the DSSC (0.65 V). The experimental operational current of the tandem system is 3.8 ± 0.6 mA/cm^2, significantly higher compared to the prediction from the photoelectrochemical analysis of single systems (3.11 mA/cm^2). The extra current measured may originate from back scattered light in the DSSC that refeeds light absorption at the CdS QDs. We also tested the device illuminating through the DSSCs (inverted configuration). However, the enhanced visible light harvesting of the N719 dye limits the operative efficiency of the QD based photoanode, and the operational current of the tandem device is significantly lower than expected, j_{sc} = 2.3 mA·cm^{-2} (see Figure S4, Supporting Information).

Moreover, STH conversion efficiency was estimated using large area devices (1.5 × 1.5 cm^2), which although less efficient than lower area devices facilitated H_2 collection. STH can be expressed as the fraction of incident solar energy photoconverted into chemical energy.[24]

$$\mathrm{STH} = \frac{j_{sc} E^0 \eta_F}{P_{total}} \qquad (2)$$

where, j_{sc} is the short-circuit current, E^0 corresponds to the thermodynamic reaction potential (0.21 V), considering that the oxidation of the sacrificial agent takes place ($\Delta G°$, = 38 600 J/mol, (see Supporting Information S6 for the detailed calculation), η_F is the faradaic efficiency of hydrogen generation in standard conditions, and P_{total} is the incident solar irradiance (W/m^2). We note that ΔG^0 is an approximation for the real ΔG involved in the reaction since our conditions are not standard and an evaluation of the activities of all the ionic species present in the electrolyte should be carried out for a more precise calculation of ΔG. However, this calculation is beyond the scope of the present work.

The evolved gas was confirmed as hydrogen in previous studies.[21] Figure 3b shows the amount of collected hydrogen in an inverted buret as a function of time, while the net photocurrent recorded during the measurement is shown in Figure S5, Supporting Information. The maximum amount of hydrogen generated can be estimated by integrating the photocurrent over the time and dividing by two since hydrogen generation is a two electron process. By comparing the experimental and theoretical plots, 100% faradaic efficiency can be safely claimed as expected due to the outstanding properties of Pt as a H_2 evolving catalyst.

STH efficiencies for both the TiO_2−CdS photoanode and the tandem device are shown in Table 1. All the measurements

Table 1. Experimental and Theoretical Solar-to-Hydrogen Conversion Efficiencies for Single TiO_2−CdS Photoanode and Tandem Device[a]

sample	J_{op} (mA·cm^{-2})	I_{op} (mA)	R_{H2} (nmol/s)	STH (%)
TiO_2-CdS	1.64 ± 0.2	0.41 ± 0.05	2.09 ± 0.26	0.34 ± 0.04
tandem	3.8 ± 0.6	0.94 ± 0.16	4.9 ± 0.8	0.78 ± 0.04

[a] J_{op}, operational current density; I_{op}, operational current; R_{H2}, rate of H_2 evolution; STH, solar-to-hydrogen conversion efficiency. See Supporting Information S6). The reported values correspond to three identical cells. The error is calculated as the standard deviation, n = 3.

were performed in standard conditions, P = 1 atm and T = 298 K, and the efficiencies were estimated for the first 1.5 h, before the consumption of sacrificial agent significantly affects the photocurrent values. In these conditions, the net current can be considered constant. This result highlights the key role of the DSSC, promoting the electron to a higher energetic state level and inducing light driven H_2 generation, with STH efficiencies of (0.78 ± 0.04)% near tripling that reported for the single QD based photoanode. To the best of the authors' knowledge, the STH conversion efficiencies reported here are the highest ones for nanostructured TiO_2 photoanodes. Additionally, the behavior of the device has showed promising stability since, as claimed in a previous study,[20] the measured decrease of the photocurrent for these QD based photoelectrodes is mainly due to the consumption of the sacrificial agent. A previous study has reported 5.5 mA/cm^2 with a tandem device based on a similar principle,[25] although STH efficiencies were not determined and the characterization and experimental details were not fully performed and explained. Another study using composite nanodispersed structures of reduced graphene oxide (RGO) QDs of solid solutions $Zn_{0.8}Cd_{0.2}S$ has showed 0.36% solar-to-hydrogen efficiency.[26]

CONCLUSIONS

In summary, we demonstrated the improvement in unassisted hydrogen generation of a CdS calchogenide photoanode by the design of a tandem device, connecting in series a ruthenium based DSSC. To the best of the authors' knowledge, the reported efficiencies are the highest ones for these heterostrutured systems. However, this study is expected to open wide avenues in the design of tailored nanocomposites based on mesoporous photoanodes working in parallel tandem devices, improving the light absorption properties within a broad spectral range, from visible to near-IR as well as hydrogen production rates. Ongoing studies in our lab are focused on the suppression of chemical bias toward the design of fully autonomous artificial photoshynthetic systems, as well as the integration of new cathode designs, which replaces platinum to balance the fabrication costs of these systems.

dx.doi.org/10.1021/jp4109893 | J. Phys. Chem. C 2014, 118, 891−895

■ ASSOCIATED CONTENT

Supporting Information

Absorption spectra of the individual components of the device, transmission electron micrograph of the TiO_2–CdS heterostructures, photovoltaic parameters of the DSSC, details of the inverted configuration of the tandem device, chronoamperometric measurement of H_2 evolution, detailed calculation of STH. This material is available free of charge via the Internet at http://pubs.acs.org.

■ AUTHOR INFORMATION

Corresponding Authors

*(I.M.-S.) E-mail: sero@uji.es.

*(S.G.) E-mail: sjulia@uji.es.

Notes

The authors declare no competing financial interest.

■ ACKNOWLEDGMENTS

We acknowledge support by project P1.1B2011-50. The SCIC of the University Jaume I de Castello is also acknowledged for the TEM measurements. We want to acknowledge Prof. J. Bisquert for the fruitful discussions related to this manuscript.

■ REFERENCES

(1) Crabtree, G. W.; Lewis, N. S. Solar Energy Conversion. *Phys. Today* **2007**, *60*, 37–42.

(2) Crittenden, J. C.; White, H. S. Harnessing Energy for a Sustainable World. *J. Am. Chem. Soc.* **2010**, *132*, 4503–4505.

(3) Barber, J. Photosynthetic Energy Conversion: Natural and Artificial. *Chem. Soc. Rev.* **2009**, *38*, 185–196.

(4) Gust, D.; Moore, T. A.; Moore, A. L. Solar Fuels Via Artificial Photosynthesis. *Acc. Chem. Res.* **2009**, *42*, 1890–1898.

(5) Chen, X.; Shen, S.; Guo, L.; Mao, S. S. Semiconductor-Based Photocatalytic Hydrogen Generation. *Chem. Rev.* **2010**, *110*, 6503–6570.

(6) Fujishima, A.; Honda, K. Electrochemical Photolysis of Water at a Semiconductor Electrode. *Nature* **1972**, *238*, 37–38.

(7) Bard, A. J.; Fox, M. A. Artificial Photosynthesis: Solar Splitting of Water to Hydrogen and Oxygen. *Acc. Chem. Res.* **1995**, *28*, 141–145.

(8) Lewis, N. S. Light Work with Water. *Nature* **2001**, *414*, 589–590.

(9) Reece, S. Y.; Hamel, J. A.; Sung, K.; Jarvi, T. D.; Esswein, A. J.; Pijpers, J. J. H.; Nocera, D. G. Wireless Solar Water Splitting Using Silicon-Based Semiconductors and Earth-Abundant Catalysts. *Science* **2011**, *334*, 645–648.

(10) Rocheleau, R. E.; Miller, E. L.; Misra, A. High-Efficiency Photoelectrochemical Hydrogen Production Using Multijunction Amorphous Silicon Photoelectrodes. *Energy Fuels* **1998**, *12*, 3–10.

(11) Weber, M. F.; Dignam, M. J. Efficiency of Splitting Water with Semiconducting Photoelectrodes. *J. Electrochem. Soc.* **1984**, *131*, 1258–1265.

(12) Weber, M. F.; Dignam, M. J. Splitting Water with Semiconducting Photoelectrodes—Efficiency Considerations. *Int. J. Hydrogen Energy* **1986**, *11*, 225–232.

(13) Khaselev, O.; Turner, J. A. A Monolithic Photovoltaic–Photoelectrochemical Device for Hydrogen Production Via Water Splitting. *Science* **1998**, *280*, 425–427.

(14) van de Krol, R.; Liang, Y.; Schoonman, J. Solar Hydrogen Production with Nanostructured Metal Oxides. *J. Mater. Chem.* **2008**, *18*, 2311–2320.

(15) Caramori, S.; Cristino, V.; Argazzi, R.; Meda, L.; Bignozzi, C. A. Photoelectrochemical Behavior of Sensitized TiO_2 Photoanodes in an Aqueous Environment: Application to Hydrogen Production. *Inorg. Chem.* **2010**, *49*, 3320–3328.

(16) Youngblood, W. J.; Lee, S.-H. A.; Maeda, K.; Mallouk, T. E. Visible Light Water Splitting Using Dye-Sensitized Oxide Semiconductors. *Acc. Chem. Res.* **2009**, *42*, 1966–1973.

(17) Hensel, J.; Wang, G.; Li, Y.; Zhang, J. Z. Synergistic Effect of Cdse Quantum Dot Sensitization and Nitrogen Doping of TiO_2 Nanostructures for Photoelectrochemical Solar Hydrogen Generation. *Nano Lett.* **2010**, *10*, 478–483.

(18) Jin-nouchi, Y.; Hattori, T.; Sumida, Y.; Fujishima, M.; Tada, H. PBS Quantum Dot-Sensitized Photoelectrochemical Cell for Hydrogen Production from Water under Illumination of Simulated Sunlight. *ChemPhysChem* **2010**, *11*, 3592–3595.

(19) Luo, J.; Karuturi, S. K.; Liu, L.; Su, L. T.; Tok, A. I. Y.; Fan, H. J. Homogeneous Photosensitization of Complex TiO_2 Nanostructures for Efficient Solar Energy Conversion. *Sci. Rep.* **2012**, *2*, 451.

(20) Rodenas, P.; Song, T.; Sudhagar, P.; Marzari, G.; Han, H.; Badia-Bou, L.; Gimenez, S.; Fabregat-Santiago, F.; Mora-Sero, I.; Bisquert, J.; et al. Quantum Dot Based Heterostructures for Unassisted Photoelectrochemical Hydrogen Generation. *Adv. Energy Mater.* **2013**, *3*, 176–182.

(21) Trevisan, R.; Rodenas, P.; Gonzalez-Pedro, V.; Sima, C.; Sanchez, R. S.; Barea, E. M.; Mora-Sero, I.; Fabregat-Santiago, F.; Gimenez, S. Harnessing Infrared Photons for Photoelectrochemical Hydrogen Generation. A PBS Quantum Dot Based "Quasi-Artificial Leaf. *J. Phys. Chem. Lett.* **2012**, *4*, 141–146.

(22) Wang, G. M.; Yang, X. Y.; Qian, F.; Zhang, J. Z.; Li, Y. Double-Sided CdS and CdSe Quantum Dot Co-Sensitized ZnO Nanowire Arrays for Photoelectrochemical Hydrogen Generation. *Nano Lett.* **2010**, *10*, 1088–1092.

(23) Herraiz-Cardona, I.; Ortega, E.; Vazquez-Gomez, I.; Perez-Herranz, V. Electrochemical Characterization of a NiCo/Zn Cathode for Hydrogen Generation. *Int J. Hydrogen Energy* **2011**, *36*, 11578–11587.

(24) Chen, Z.; Jaramillo, T. F.; Deutsch, T. G.; Kleiman-Shwarsctein, A.; Forman, A. J.; Gaillard, N.; Garland, R.; Takanabe, K.; Heske, C.; Sunkara, M.; et al. Accelerating Materials Development for Photoelectrochemical Hydrogen Production: Standards for Methods, Definitions, and Reporting Protocols. *J. Mater. Res.* **2010**, *25*, 3–16.

(25) Shin, K.; Yoo, J.-B.; Park, J. H. Photoelectrochemical Cell/Dye-Sensitized Solar Cell Tandem Water Splitting Systems with Transparent and Vertically Aligned Quantum Dot Sensitized TiO_2 Nanorod Arrays. *J. Power Sources* **2013**, *225*, 263–268.

(26) Zhang, J.; Yu, J. G.; Jaroniec, M.; Gong, J. R. Noble Metal-Free Reduced Graphene Oxide-$Zn_xCd_{1-x}S$ Nanocomposite with Enhanced Solar Photocatalytic H_2-Production Performance. *Nano Lett.* **2012**, *12*, 4584–4589.